




Soliton macromolecule dynamics in fiber lasers with sinusoidal filtered nonlinear optical loop mirrorZengrun Wen ^{1,2} Weiming Wang,^{1,2} Song Gao ^{1,2} Kaile Wang ³ Yangjian Cai,^{1,2} and Yuanmei Gao^{1,2,*}¹*Center of Light Manipulations and Applications & Shandong Provincial Key Laboratory of Optics and Photonic Device, Shandong Normal University, Jinan, 250014, China*²*School of Physics and Electronics, Shandong Normal University, Jinan 250014, China*³*The State Key Laboratory of Integrated Service Networks, The School of Telecommunications Engineering, Xidian University, Xi'an 710071, China*

(Received 20 April 2022; revised 19 August 2022; accepted 23 August 2022; published 30 August 2022)

We numerically investigated the pulse dynamics of soliton macromolecules (SMs) in erbium-doped fiber lasers mode-locked using a nonlinear optical loop mirror (NOLM) with a sinusoidal spectral filter (SSF). SM regimes with various pulse intervals were proposed by modulating the saturation energy and filter period, distributed discretely owing to the restriction of the cavity length and pulse-to-pulse interaction. Several SM properties were discovered in stable SM states with filter periods of 1.3 and 1.95 nm, including the π -phase difference between adjacent pulses, Kelly sidebands in optical spectra, and the alternating change of phases against round trips. The laser worked in transition regimes, such as pulse splitting and pulsating to a stable SM, by increasing the saturation energy with certain filter periods. In pulsating SM regimes, soliton collisions and periodic variations of pulse intervals and peak powers occurred, accompanied by energy transfer between different spectrum components or spectrum shifts. This study reveals that the SSF-based NOLM enables SM generation and provides a method for controlling the SM dynamics in fiber lasers.

DOI: [10.1103/PhysRevA.106.023522](https://doi.org/10.1103/PhysRevA.106.023522)**I. INTRODUCTION**

An optical soliton is a type of solitary wave formed through the balance of anomalous dispersion and Kerr nonlinearity [1]. In fiber lasers operating in an anomalous dispersion regime, solitons also experience gain and cavity loss, possessing Kelly sidebands on the two sides of the central wavelength owing to the oscillation of the dispersive waves, which are known as conventional solitons [2]. During the increase in pump power or polarization modulation, the soliton can split and form a bound state, also known as a soliton molecule, in which two or more solitons are bound together with some fixed pulse intervals and identical pulse properties [3–5]. Over the last two decades, a variety of intriguing stable and unstable solitons have been theoretically predicted and experimentally discovered in fiber lasers with different configurations [6]. To investigate the generation of these solitons and their interactions, many rigorous numerical models based on the Ginzburg-Landau equation for fibers and dispersive Fourier transform technology have been utilized to promote the development of fiber lasers that generate ultrafast pulses with high peak power, stable lasing with a high repetition rate, and other desired pulses [7–10]. Simultaneously, as a type of dissipative nonlinear system, fiber lasers enable the study of complex soliton behaviors beyond stable solitons, such as pulsating solitons, soliton explosions, breather solitons, shaking soliton molecules, and multipulse instability, thereby providing

insight into the nonlinear process with non-Hermitian modulations [11–15].

In addition to small soliton molecules comprising two or three solitons, there are soliton macromolecules (SMs) with a sequence of tens or even hundreds of long-range interacting solitons and soliton crystals, characterized by an array of regularly distributed solitons in the temporal domain [16,17]. Such a large number of solitons, analogous to their chemical counterparts or beyond, also have potential applications in high-speed optical communications [18], achieving controllable high-order harmonic mode-locking pulses [19], spectroscopy [20], and optical ranging [21]. Therefore, it is reasonable to understand the formation and physical dynamics of large-scale soliton molecules. Recently, soliton crystals have been commonly realized in microresonators [22,23], but they have rarely been realized in mode-locked fiber lasers with long cavity lengths [16]. In general, SMs are generated in nonlinear polarization rotation fiber lasers because of slow gain recovery and depletion, which occupy a local range of one cavity length [24–26]. In addition, the optomechanical or Casimir-like effect can be utilized to form SMs by commanding long-range interactions between solitons [27,28]. As another important fast saturable absorber, the nonlinear optical loop mirror (NOLM) also supports the generation of small soliton molecules [29,30] and several unequal-spaced multi-bound solitons in standard figure-of-eight fiber lasers [31,32]. To form stable SMs or soliton crystals in NOLM lasers, an extra comb filter, such as the Mach-Zehnder interferometer, is necessary [33]. Considering the critical role of filtering in pulse shaping, a theoretical model of sinusoidal spectral filtering (SSF) on soliton dynamics was systematically investigated

*gaoyuanmei@sdnu.edu.cn

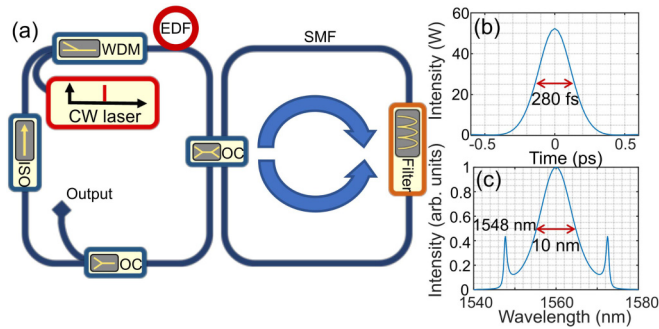


FIG. 1. (a) Schematic of NOLM fiber laser with sinusoidal filter. EDF, erbium-doped fiber laser; SMF, single-mode fiber; WDM, wavelength division multiplex; OC, optical coupler; ISO, isolator. (b) Pulse intensity and (c) normalized optical spectrum generated by the NOLM laser without a filter.

in a dispersion-management erbium-doped fiber laser [34]. However, the effect of SSF on the NOLM laser configuration remains an open topic. In addition, the formation and evolution of SM dynamics have never been revealed under the modulation of SSF, and the behaviors of SMs in figure-of-eight fiber lasers also need to be systematically explored.

In this study, the generation and modulation of SMs in a fiber laser mode-locked by an SSF-based NOLM are numerically investigated. To analyze the evolution dynamics of SM in the laser, a lumped theoretical model based on the scalar nonlinear Schrödinger equation and the transmittance of cavity devices is created. The double-parameter scanning approach is used to label the area of SM states during the change in saturation energy and filter period to provide all characteristics. The SM features, such as pulse intensities, phases, and optical spectra, are studied in detail. In addition, a detailed transition of the SM regimes to saturation energy and pulsating states is proposed.

II. THEORETICAL MODEL

To draw near the practical conditions, we erect a theoretical pulse-tracing model based on a typical figure-of-eight fiber laser with a ring cavity and a coupler-connected NOLM mode-locker. As shown in Fig. 1, the numerical model follows a pulse trajectory. For quick convergence, the starting pulse is set to a weak Gaussian signal rather than white noise. The pulse propagates through an erbium-doped fiber (EDF) and splits into two parts after an optical coupler (OC). Thereafter, the two pulses are transmitted in the NOLM bidirectionally and converge to a pulse after the asymmetric phase shift, propagating in the main loop in the clockwise direction. Finally, the pulse returns to the EDF through the output OC. The isolator (ISO) guarantees unidirectional transmission of the main loop, whose function is simulated by ignoring the counterclockwise pulse energy. A tunable SSF is deployed in the NOLM and acts as a Lyot filter, a comb filter, Mach-Zehnder interferometer, or a Sagnac interferometer [35]. All components in the cavity are connected by single-mode fibers (SMFs), and each is considered individually. To describe the pulse propagation in the fiber, a scalar Ginzburg-Landau

equation is employed:

$$\frac{\partial A}{\partial z} = i\frac{\beta_2}{2}\frac{\partial^2 A}{\partial t^2} + i\gamma|A|^2A + g(z)A + \frac{g(z)}{\Omega_g^2}\frac{\partial^2 A}{\partial t^2}, \quad (1)$$

where A , β_2 , γ , and Ω_g represent the pulse envelope, the second-order dispersion, the nonlinear coefficient, and the gain bandwidth, respectively. Variable $g(z)$ is the gain of the EDF, whose value is zero for the SMF. Considering the saturable gain condition, $g(z)$ has the following form:

$$g(z) = g_0 \exp(E_p/E_{\text{sat}}), \quad (2)$$

where g_0 is the small-signal gain coefficient, and E_p represents the pulse energy and temporal integral of the pulse intensity. The variation in pump power is delegated by altering the value of the saturation energy E_{sat} , whereas g_0 remains invariant because of its small range of variation during the process.

An SSF is inserted in an asymmetrical position of the NOLM with the following expression:

$$H(\omega) = \frac{1}{2} \left[1 - \cos\left(\frac{\omega - \omega_0}{\Omega}\right) \right], \quad (3)$$

where ω and ω_0 are the angular frequency and the central angular frequency (representing the central wavelength of 1560 nm in this study), respectively. The filter period is characterized by the value of Ω .

In the theoretical model, Eq. (1) was numerically resolved using the symmetric split-step Fourier transform method. The simulation for the stable pulse regimes converged universally within several hundred round trips. Therefore, it is reasonable to terminate the simulation after 2000 round trips.

To precisely express the effect of SSF, instead of the commonly used transfer function of NOLM [36], we employ a pulse-tracing method, thereby enabling us to consider the SSF individually.

All the simulation parameters refer to the data from the experimental setups for the erbium-doped fiber laser: $\beta_2 = 29.53 \text{ ps}^2/\text{km}$, $\gamma = 3.0 \text{ W}^{-1} \text{ km}^{-1}$, $g_0 = 3$, and $\Omega_g = 30 \text{ nm}$ for the EDF; $\beta_2 = -23.0 \text{ ps}^2/\text{km}$ and $\gamma = 1.3 \text{ W}^{-1}$ for the SMF; the saturation energy $E_{\text{sat}} = 10\text{--}500 \text{ pJ}$; and $\Omega = 0.05\text{--}3 \text{ nm}$ for the SSF. The coupling coefficient of the two OCs was 30:70 and the lengths of the EDF and the SMF were 1 and 5 m, respectively. The cavity length was 6 m, which corresponds to a one cavity round-trip time of 30 ns. For fast convergence, the range of the fast time t was set to 100 ps (-50 to 50 ps). The total dispersion of the cavity was calculated as -0.085 ps^2 ; thus, the laser operated in the anomalous dispersion regime.

III. RESULTS AND DISCUSSIONS

For comparison, SSF was not considered in the first simulation. Figures 1(b) and 1(c) show the pulse intensity and the optical spectrum, respectively, with a saturation energy of 200 pJ. The two iconic Kelly sidebands located at 1548 and 1572 nm classify the pulse as a conventional soliton. The pulse duration and the spectrum width were 280 fs and 10 nm, respectively; therefore, the soliton was chirped.

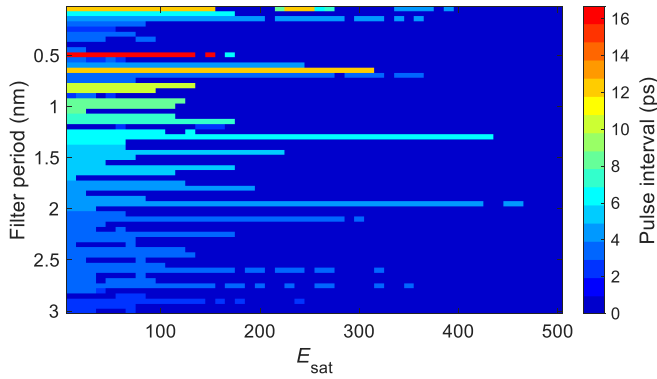


FIG. 2. Pulse intervals of SMs versus saturation energy E_{sat} and the filter period. The zero area marked as dark blue (dark gray) represents the chaotic state with unequal pulse peak power.

A. Statistical area of SM in double-parameter space

To investigate the effect of SSF in the laser, the double-parameter scanning method was used to display the SM area with the variation of the filter period (vertical axis) and the saturation energy, E_{sat} (horizontal axis), as shown in Fig. 2. By calculating the standard deviation of the pulse peak power, if the value is less than 10^{-4} , the pulse is characterized as an SM, which contains both stable and pulsating states. We employ an identification method based on the pulse properties of the bound states and SM characteristics [37]. The dark-blue (dark-gray) areas in Fig. 2 label chaotic states with different pulse intensities in a sequence. SM states exist for almost all filter periods at a small value of E_{sat} , whereas only some specific filter periods support SMs for large E_{sat} . This arises from the Kerr nonlinearity enhanced soliton interaction in the SMs. This interaction between solitons in bound states results in the discretization of the pulse spacing in fiber lasers [38]. The principle that a low pump power contributes to SM access has been revealed in microresonators [17]. The pulse interval of SMs is depicted by colors, which distribute discontinuously as a function of the filter period because of the limitation of the boundary condition (representing the cavity condition). In addition, SMs with identical pulse intervals are generated within a small range of filter periods. If the filter period is larger than 0.8 nm, the pulse interval is reduced monotonously, corresponding to an increasing number of solitons in one cavity round trip. In this area, discrete pulse intervals determine the corresponding fixed spacing of the spectral peaks. Therefore, the SMs are stable in the laser once the filter period equals the spectral spacing, such as in four remarkable examples with filter periods of 1.3, 1.45, 1.95, and 2.1 nm. With filter periods of less than 0.8 nm, there is a complex change in pulse intervals, which indicates that there is an inconformity between the filter period and the spacing of spectral peaks. When the filter period was 0.5 nm, the largest pulse interval of the SMs in the entire simulation was generated. The minimum pulse interval occurred with a filter period of 0.25 nm, which is identical to the case with a filter period of approximately 2.9 nm. By increasing E_{sat} with increments of 10 pJ, the SM states are not continuous because of the difficult balance between soliton interaction, filtering, gain, and loss. However, the pulse intervals remained invariant for almost all fixed filter

periods. However, the condition changed with four specific filter periods of 0.05, 0.5, 0.55, and 0.9 nm, where the pulse intervals were altered, indicating the transition state of the SMs.

B. Pulse characteristics of stable SMs

By scanning the two variables of the filter period and E_{sat} , the pulse characteristics of the SMs are concretely determined. First, we focus on stable SMs and enumerate two filter periods of 1.3 and 1.95 nm. Correspondingly, the pulse intensities, phases, and optical spectra for four different E_{sat} are displayed in Fig. 3. Every pulse train of the SMs contains a series of pulses with uniform spacing, identical peaks, and pulse durations. In addition, the pulse intervals remained invariant with increasing E_{sat} , which were 6.25 and 4.17 ps, respectively. In this process, the pulse duration is narrowed and the range of the optical spectrum is broadened. The optical spectra comprise equally spaced peaks with gradual symmetric energy attenuation versus the spectrum away from the center wavelength, which is a typical characteristic of perfect SMs [39]. According to the relation between the temporal duration and the spectral interval, the calculated spacing of spectral intervals is 1.3 and 1.95 nm, respectively, which are the same as the filter periods. However, in contrast to the perfect SMs in microresonators, sideband peaks located at the envelopes of the spectral peaks appear with increasing E_{sat} , as shown in Figs. 3(b2)–3(b4), whose inducement is the same as that of the Kelly sidebands, resulting from the resonance of solitons and dispersive waves. As increasing E_{sat} , there were more peaks and dips in the peak envelopes. For the filter period of 1.95 nm, the sideband on the peak envelope is less apparent than that of the counterparts with a filter period of 1.3 nm. This is because the larger filter period induced more pulses in one round trip, reducing their peak powers and thereby weakening the Kerr nonlinearity. In addition, the phases of the stable SMs were simulated, as depicted by the red lines in Figs. 3(a1)–3(a4) and 3(c1)–3(c4) for both filter periods. For the case of $E_{\text{sat}} = 100$ pJ and a filter period of 1.3 nm, the phase is distributed alternatively as periodic rectangular waves along the pulse train, and the phase difference between the adjacent pulses is π . Note that this π -phase difference is restrained by filtering this type of SSF. The abrupt transition of the phases occurs in the middle of every two pulses. As investigated in Refs. [40,41], the solitons in the bound state with phase differences of 0, $\pi/2$, and π can stably propagate in fiber lasers, whereas the soliton molecule with a π -phase difference is difficult to maintain because of the repulsion between the solitons [42]. However, in SM regimes, such repulsions can be mutually canceled in equally spaced ensembles. From the inset of Fig. 3(a1), the phases in the spatiotemporal evolution present a checkerboard pattern, indicating that the phase period of the pulses in the SMs is two cavity round trips. For a larger E_{sat} , the phases at the pulse peaks hump up simultaneously and maintain the π -phase difference between neighboring pulses [Fig. 3(a2)]. In Fig. 3(a3), the phase change exceeds π during the transition time. When we set $E_{\text{sat}} = 400$ pJ, there was a decreasing oscillation of the phase between two adjacent pulses after the phase transition. The above phase variations indicate that a more complicated

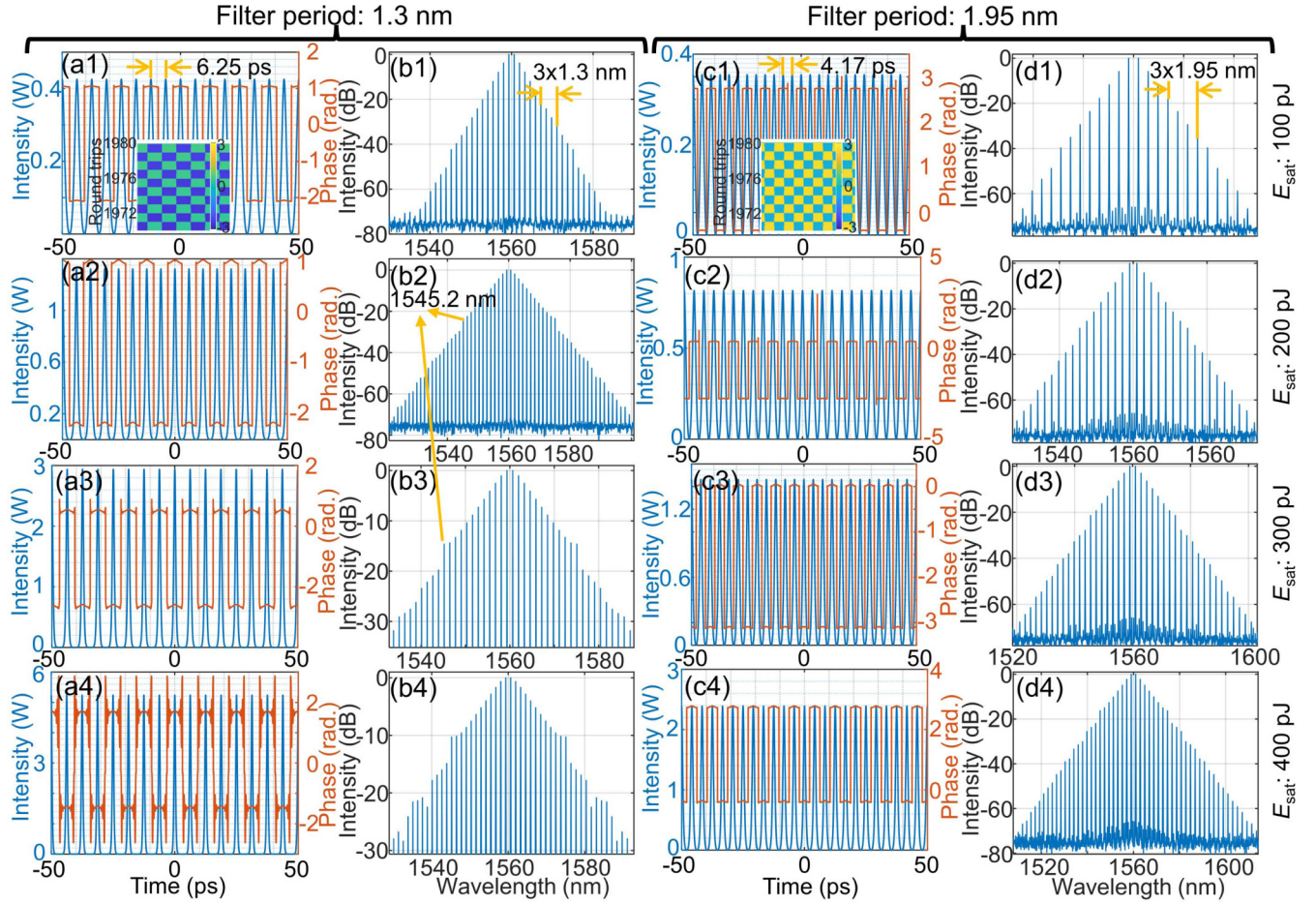


FIG. 3. Pulse intensities, phases and optical spectra of stable SMs with different filter periods and E_{sat} . (a1–a4) Pulse intensities and (b1–b4) optical spectra with the filter period of 1.3 nm, respectively. Panels (c1–c4) and (d1–d4) are the same as panels (a1–a4) and (b1–b4) with a filter period of 1.95 nm. Red lines in panels (a1–a4) and (c1–c4) represent the corresponding phase curves. The insets of panels (a1) and (c1) are the local phase evolutions with the change of round trip.

chirp is generated during the up-process of E_{sat} . However, all phases are distributed as rectangular waves for a filter period of 1.95 nm because of the lower peak powers.

C. Transition of SM regimes with respect to E_{sat}

In the statistical map of SMs, four filter periods support the change in the pulse intervals. Two of the four filter periods are selected to investigate the pulse transitions, which are 0.05 and 0.5 nm, as shown in Figs. 4(a1)–4(a3) and 4(b1)–4(b3), respectively. When E_{sat} is 100 pJ, the pulse duration of the SM first broadens and narrows and finally reaches a stable SM regime [Fig. 4(a1)]: Once E_{sat} is raised to 220 pJ, each pulsating pulse of the SM splits into two pulses with identical phases synchronously after ~ 180 round trips. Then, the splinters mutually attract to constitute one pulsating soliton again and repeat the next splitting [Fig. 4(a2)]: Upon further increasing the pump power, the laser experiences chaotic states and finally reaches a steady SM state with $E_{\text{sat}} = 340$ pJ. As depicted in Fig. 4(a3), each initial pulse is split into unstable double pulses that attract and form a single pulse. Consequently, the pulse split into three pulses and became stable as it circulated in the cavity. The newly generated SM contains a series of pulses with the π -phase difference

between their neighbors; however, the pulse interval becomes one-third of that in Fig. 4(a1): From the inset of Fig. 4(a3), there are two types of peaks with 20-dB intensity difference in the optical spectrum. In addition, the interval of the higher peak train is triple that of the lower peak train, which indicates that the intensity of the new SM is weakly modulated. When the filter period was 0.5 nm, the laser rapidly reached a stable SM state with low pump power, as shown in Fig. 4(b1): With a higher E_{sat} , the laser operates in a pulsating SM state, whose formation is similar to that of a single pulsating soliton. In contrast, the energy of the optical spectrum is transferred periodically between different filtering frequencies [inset of Fig. 4(b2)]: If E_{sat} is set to 170 pJ, each pulse of the SM is split into two pulses with identical phase distributions. The splinters from two adjacent initial pulses approached each other and were located at different fixed times, forming a new pulse regime with alternatively spaced solitons. This distribution is the same as the one-dimensional topological Su-Schrieffer-Heeger model [43]. Correspondingly, the peaks of the optical spectrum are modulated owing to the nonuniform soliton spacing [inset of Fig. 4(b3)]. In addition, there was another transition state of the SM without pulse splitting; as shown in Figs. 4(c1)–4(c3), the pulsating SM transforms into a high-pulsating SM and finally stabilizes with increasing

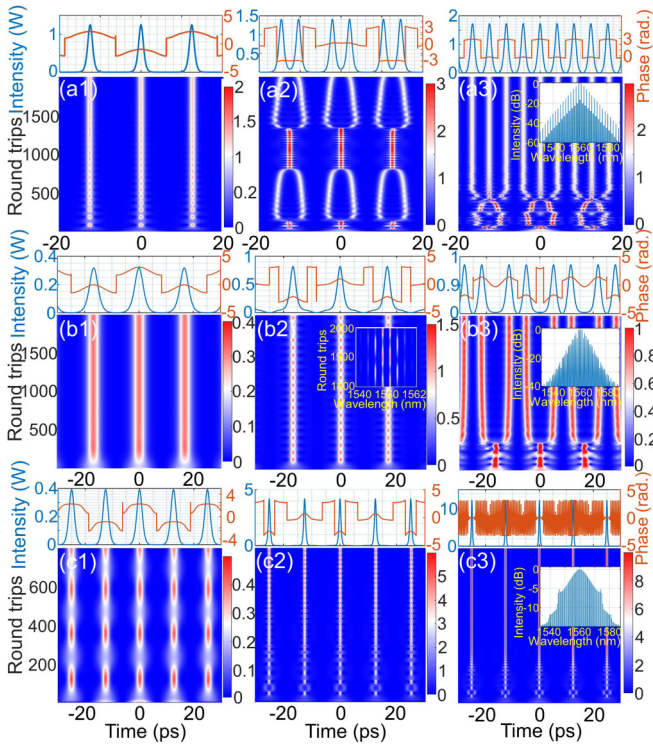


FIG. 4. Transition of SM regimes. (a1–a3) Splitting of SM with E_{sat} values of 100, 220, and 340 pJ, respectively, accompanied by a filter period of 0.05 nm. (b1–b3) Transition from stable SM to pulsating SM to alternatively spaced SM with increasing E_{sat} values of 50, 100, and 170 pJ, respectively, when the filter period is 0.5 nm. (c1–c3) Transition from pulsating SM to stable SM by setting E_{sat} as 50, 200, and 300 pJ, respectively, with the corresponding filter period of 0.65 nm. The insets of panels (a3), (b3), and (c3) are the corresponding optical spectra. The inset of panel (b2) is the evolution of the optical spectrum from 1800 to 2000 round trips.

E_{sat} . The solitons of the stable SM are narrowed because of the Kerr nonlinearity. Correspondingly, the phase oscillates violently between the two solitons, whereas the π -phase difference is maintained for the phases at two adjacent pulse peaks. From the inset of Fig. 4(c3), there are sidebands on the envelope of the spectral peaks, indicating that the SM consists of conventional solitons.

D. Pulsating SM regimes

Apart from stable and transition SMs, there are pulsating SMs in which the solitons collide and intervene with their neighbors, inducing the periodic alteration of soliton intervals and peak powers with respect to round trips, as shown in Fig. 5. In a fiber laser, the pulsating state often occurs in the transition range of pulse regimes during pump power growth [44], as discussed in the previous section. Here, the pulsating states are caused by the filtering effect. When the filter period mismatches the interval of spectral peaks, filtering influences the locations of the spectral peaks, resulting in the alteration of solitons in group velocities [45]. Figure 5(a) shows the spatiotemporal evolution of a pulsating SM with $E_{\text{sat}} = 50$ pJ and a filter period of 0.4 nm. In the time region of -30 to 30 ps, the initial weak signal forms three solitons, each of which splits

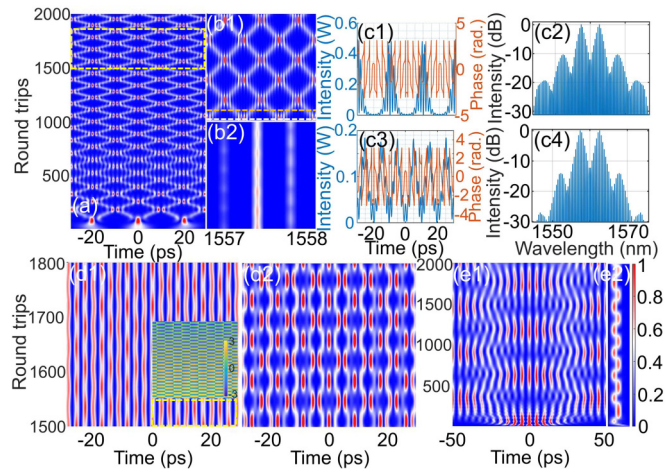


FIG. 5. Pulsating SMs under different E_{sat} values and filter periods. (a) Spatiotemporal pattern of pulse intensity at $E_{\text{sat}} = 50$ pJ and a filter period of 0.4 nm. Partial magnified view of the pulse intensity (b1) and the optical spectrum (b2) of panel (a). Panels (c1–c2) and (c3–c4) are pulse intensities and optical spectra at 1500 and 1550 round trips, respectively. (d1) and (d2) Evolution of pulse intensities at $E_{\text{sat}} = 50$ and 200 pJ, respectively, accompanied by a filter period of 0.9 nm. Transmission of (e1) pulse intensity and (e2) local spectrum with $E_{\text{sat}} = 100$ pJ and a filter period of 1.7 nm.

into two solitons with opposite group velocities. The solitons collide with counterparts generated by their neighbors and change the group velocity. After approximately 1200 round trips, a stable periodic soliton collision occurs. By enlarging the area of 1500–1800 round trips, there is an obvious interference fringe in the collision area, as shown in Fig. 5(b1). In addition, the left maximum spectral peak increases corresponding to soliton collision [Fig. 5(b2)]. Figures 5(c1)–5(c4) show the pulse intensities, phases, and spectra at 1500 and 1550 round trips. The interference fringe indicates the inverse phase of adjacent solitons. In the frequency domain, a dip is located at the central wavelength and there are several sidebands on the spectral peaks that constitute the envelopes. In addition, in the noncollision area, the intensities of the sidebands are lowered for the maximum-intensity sidebands. When the filter period is 0.9 nm, instead of soliton collisions, the splitting solitons attract and repel adjacent solitons, forming oscillations of the peak powers [Fig. 5(d1)]. Under these circumstances, all the phases change gradually with the same pulse pulsation period, as shown in the inset of Fig. 5(d1). By increasing E_{sat} to 200 pJ, the attraction and repulsion between the solitons become more obvious. If the filter period is larger, sufficient space is provided for the spectral peak shift in one filtering window. As shown in Figs. 5(e1) and 5(e2), the maximum spectral peak shifts abruptly for every change in the group velocity direction. This phenomenon is similar to the total reflection of pulses at temporal waveguide interfaces [46,47].

E. Chaotic SMs and long-term stability

In Sec. III A, chaotic states are represented by the dark-blue (dark-gray) area in Fig. 2. When the filter period and the saturation energy are set as 1.5 nm and 300 pJ, respectively,

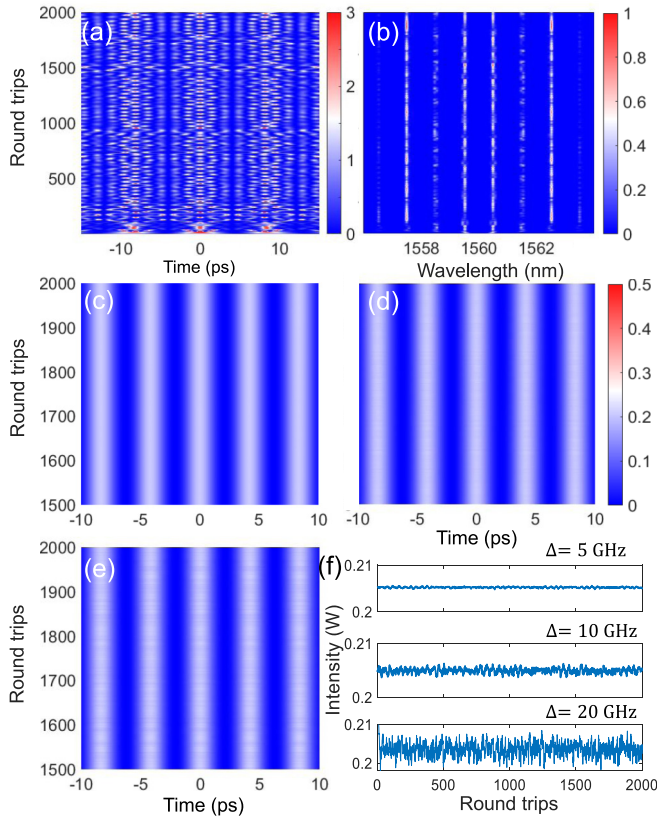


FIG. 6. Pulse dynamics of chaotic SM states and long-term instability. (a) Spatial-temporal evolution of the pulse intensity and (b) spectrum of the laser with a filter period of 1.5 nm and $E_{\text{sat}} = 300$ pJ. (c)–(e) Evolution of pulse intensities of the laser with the filter period randomly altered within 5, 10, and 20 GHz, respectively. (f) Peak intensities correspond to panels (c)–(e).

the mode-locking cannot reach a steady state, and as shown in Figs. 6(a) and 6(b), the pulse splits and assembles irregularly as it cycles in the cavity. Correspondingly, several components of the spectrum emerge and disappear. In the chaotic state, mode-locking is unbalanced under the combined action of soliton interaction and spectral filtering, which is caused by increasing the saturation energy (enhancing the soliton interaction) or changing the filter period. Once stable mode-locking is formed, the laser is robust to a certain disturbance [48,49]. However, the alteration of intracavity elements can also change the uniformity of mode-locking over time, that is,

the long-term stability of the laser. To numerically simulate the degree of robustness, the period of the SF was altered randomly within a certain range, and the pulse propagation was monitored simultaneously. In the simulation, the filter period and the saturation energy were 1.95 nm and 200 pJ, respectively. When the filter period is randomly changed between 5 GHz (1.91–1.99 nm) and 10 GHz (1.91–1.99 nm), the pulses are relatively stable with peak power fluctuations of 0.4% and 1.27%, respectively. If the random degree of the filter period is raised to 20 GHz (1.87–2.03 nm), the pulse peak is disturbed severely and the mode-locking is transformed into a chaotic state, as depicted in Figs. 6(c)–6(f), respectively.

IV. CONCLUSIONS

The SM dynamics in a fiber laser mode-locked using an SSF-based NOLM were numerically investigated. The lumped numerical model of the laser considers the pulse evolution in the NOLM with a tunable SSF. By altering the saturation energy and the filter period, various SM behaviors, including stable SMs, transition SMs, and pulsating SMs, are obtained, indicating that the discrete SM distribution originates from the interactions of quantum intervals of bound solitons and the filtering effect. In stable SMs, there is a π -phase difference between the adjacent solitons, and Kelly sidebands emerge with an increase in pump power. In addition, three transition regimes under small filter periods are achieved by increasing the pump power: stable SM to SM splitting, the transition from stable SM to pulsating SM to alternatively spaced SM, and pulsating SM to stable SM. Furthermore, the mismatch between the filter period and the spectral peak positions determined by soliton interaction leads to periodic collision and variation of soliton intervals, namely, pulsating SMs. The chaotic SMs and the long-term stability of a stable SM were also investigated. This study investigated the effect of sinusoidal filtering in an NOLM on the SM dynamics in fiber lasers, paving the way for generating SMs in fiber lasers. This method can be easily extended to other types of fiber lasers with different wavelengths or dispersion regimes.

ACKNOWLEDGMENTS

We acknowledge the support of the National Natural Science Foundation of China (Grants No. 12104272, No. 91950104, No. 12147155, and No. 12104265).

[1] G. P. Agrawal, *Nonlinear Fiber Optics*, 5th ed. (Academic Press, Boston, 2013).
 [2] L. M. Zhao, D. Y. Tang, H. Zhang, X. Wu, and N. Xiang, Soliton trapping in fiber lasers, *Opt. Express* **16**, 9528 (2008).
 [3] D. Y. Tang, W. S. Man, H. Y. Tam, and P. D. Drummond, Observation of bound states of solitons in a passively mode-locked fiber laser, *Phys. Rev. A* **64**, 033814 (2001).
 [4] Z. Q. Wang, K. Nithyanandan, A. Coillet, P. Tchofo-Dinda, and P. Grelu, Optical soliton molecular complexes in a passively mode-locked fibre laser, *Nat. Commun.* **10**, 830 (2019).

[5] L. Nimmegern, C. Beckh, H. Kempf, A. Leitenstorfer, and G. Herink, Soliton molecules in femtosecond fiber lasers: Universal binding mechanism and direct electronic control, *Optica* **8**, 1334 (2021).
 [6] R. I. Woodward, Dispersion engineering of mode-locked fibre lasers, *J. Opt.* **20**, 033002 (2018).
 [7] Y. Du, C. Zeng, Z. He, Q. Gao, D. Mao, and J. Zhao, Trampoline-like pulsating soliton fiber lasers, *Phys. Rev. A* **104**, 023503 (2021).
 [8] X. Li, S. Zhang, J. Liu, and Z. Yang, Efficient method to improve the distribution probability of dissipative

- soliton and noise-like pulse in all-normal-dispersion fiber lasers, *Opt. Express* **30**, 6161 (2022).
- [9] S. Liu, T. Cao, J. Yan, K. Hu, Z. Guo, Z. Liu, Q. Xu, Z. Li, and J. Peng, Single-shot method to study high order solitons in all-polarization-maintaining soliton mode-locked fiber lasers, *Opt. Express* **29**, 38337 (2021).
- [10] Y. Zhou, Y.-X. Ren, J. Shi, H. Mao, and K. K. Y. Wong, Buildup and dissociation dynamics of dissipative optical soliton molecules, *Optica* **7**, 965 (2020).
- [11] H.-J. Chen, Y.-J. Tan, J.-G. Long, W.-C. Chen, W.-Y. Hong, H. Cui, A.-P. Luo, Z.-C. Luo, and W.-C. Xu, Dynamical diversity of pulsating solitons in a fiber laser, *Opt. Express* **27**, 28507 (2019).
- [12] A. F. J. Runge, N. G. R. Broderick, and M. Erkintalo, Observation of soliton explosions in a passively mode-locked fiber laser, *Optica* **2**, 36 (2015).
- [13] J. Peng, S. Boscolo, Z. Zhao, and H. Zeng, Breathing dissipative solitons in mode-locked fiber lasers, *Sci. Adv.* **5**, eaax1110 (2019).
- [14] J. Igbonacho, K. Nithyanandan, K. Krupa, P. T. Dinda, P. Grelu, and A. B. Moubissi, Dynamics of distorted and undistorted soliton molecules in a mode-locked fiber laser, *Phys. Rev. A* **99**, 063824 (2019).
- [15] C.-H. Wu, Y. Yao, Y. Yang, X.-C. Xu, J.-J. Tian, and K. Xu, Wavelength-switchable and multi-pulse bound state based on a hybrid mode-locked mechanism, *Opt. Express* **30**, 10732 (2022).
- [16] P. Grelu and N. Akhmediev, Dissipative solitons for mode-locked lasers, *Nat. Photonics* **6**, 84 (2012).
- [17] M. Karpov, M. H. P. Pfeiffer, H. Guo, W. Weng, J. Liu, and T. J. Kippenberg, Dynamics of soliton crystals in optical microresonators, *Nat. Phys.* **15**, 1071 (2019).
- [18] P. Marin-Palomo, J. N. Kemal, M. Karpov, A. Kordts, J. Pfeifle, M. H. P. Pfeiffer, P. Trocha, S. Wolf, V. Brasch, M. H. Anderson, R. Rosenberger, K. Vijayan, W. Freude, T. J. Kippenberg, and C. Koos, Microresonator-based solitons for massively parallel coherent optical communications, *Nature (London)* **546**, 274 (2017).
- [19] C. Lecaplain and P. Grelu, Multi-gigahertz repetition-rate-selectable passive harmonic mode locking of a fiber laser, *Opt. Express* **21**, 10897 (2013).
- [20] M.-G. Suh, Q.-F. Yang, K. Y. Yang, X. Yi, and K. J. Vahala, Microresonator soliton dual-comb spectroscopy, *Science* **354**, 600 (2016).
- [21] M.-G. Suh and K. J. Vahala, Soliton microcomb range measurement, *Science* **359**, 884 (2018).
- [22] T. Huang, J. Pan, Z. Cheng, G. Xu, Z. Wu, T. Du, S. Zeng, and P. P. Shum, Nonlinear-mode-coupling-induced soliton crystal dynamics in optical microresonators, *Phys. Rev. A* **103**, 023502 (2021).
- [23] Z. Lu, H.-J. Chen, W. Wang, L. Yao, Y. Wang, Y. Yu, B. E. Little, S. T. Chu, Q. Gong, W. Zhao, X. Yi, Y.-F. Xiao, and W. Zhang, Synthesized soliton crystals, *Nat. Commun.* **12**, 3179 (2021).
- [24] A. Haboucha, H. Leblond, M. Salhi, A. Komarov, and F. Sanchez, Coherent soliton pattern formation in a fiber laser, *Opt. Lett.* **33**, 524 (2008).
- [25] A. Haboucha, H. Leblond, M. Salhi, A. Komarov, and F. Sanchez, Analysis of soliton pattern formation in passively mode-locked fiber lasers, *Phys. Rev. A* **78**, 043806 (2008).
- [26] A. Zaviyalov, P. Grelu, and F. Lederer, Impact of slow gain dynamics on soliton molecules in mode-locked fiber lasers, *Opt. Lett.* **37**, 175 (2012).
- [27] W. He, M. Pang, D. H. Yeh, J. Huang, C. R. Menyuk, and P. S. J. Russell, Formation of optical supramolecular structures in a fibre laser by tailoring long-range soliton interactions, *Nat. Commun.* **10**, 5756 (2019).
- [28] K. Sulimany, O. Lib, G. Masri, A. Klein, M. Fridman, P. Grelu, O. Gat, and H. Steinberg, Bidirectional Soliton Rain Dynamics Induced by Casimir-Like Interactions in a Graphene Mode-Locked Fiber Laser, *Phys. Rev. Lett.* **121**, 133902 (2018).
- [29] F. Amrani, M. Salhi, P. Grelu, H. Leblond, and F. Sanchez, Universal soliton pattern formations in passively mode-locked fiber lasers, *Opt. Lett.* **36**, 1545 (2011).
- [30] F. Bahloul, M. Salhi, K. Guesmi, F. Sanchez, and R. Attia, Numerical demonstration of generation of bound solitons in figure of eight microstructured fiber laser in normal dispersion regime, *Opt. Commun.* **311**, 282 (2013).
- [31] A. Kokhanovskiy, E. Kuprikov, and S. Kobtsev, Single- and multi-soliton generation in figure-eight mode-locked fibre laser with two active media, *Opt. Laser Technol.* **131**, 106422 (2020).
- [32] R. Zhou, X. Liu, D. Yu, Q. Li, and H. Y. Fu, Versatile multi-soliton patterns of noise-like pulses in a passively mode-locked fiber laser, *Opt. Express* **28**, 912 (2020).
- [33] A. Andrianov and A. Kim, Widely stretchable soliton crystals in a passively mode-locked fiber laser, *Opt. Express* **29**, 25202 (2021).
- [34] K. Zhao, X. Xiao, and C. Yang, Sinusoidal spectral filtering-based soliton dynamics in mode-locked fiber lasers, *IEEE J. Sel. Top. Quantum Electron.* **28**, 1100109 (2022).
- [35] L. Wei, X. Xu, A. Khattak, and B. Henley, Continuously tunable comb filter based on a high-birefringence fiber loop mirror with a polarization controller, *J. Lightwave Technol.* **39**, 4800 (2021).
- [36] A. Malfondet, A. Parriaux, K. Krupa, G. Millot, and P. Tchofo-Dinda, Optimum design of NOLM-driven mode-locked fiber lasers, *Opt. Lett.* **46**, 1289 (2021).
- [37] X. M. Liu, X. X. Han, and X. K. Yao, Discrete bisoliton fiber laser, *Sci. Rep.* **6**, 34414 (2016).
- [38] G. Herink, F. Kurtz, B. Jalali, D. R. Solli, and C. Ropers, Real-time spectral interferometry probes the internal dynamics of femtosecond soliton molecules, *Science* **356**, 50 (2017).
- [39] D. C. Cole, E. S. Lamb, P. Del'Haye, S. A. Diddams, and S. B. Papp, Soliton crystals in Kerr resonators, *Nat. Photonics* **11**, 671 (2017).
- [40] L. Gui, X. Xiao, and C. Yang, Observation of various bound solitons in a carbon-nanotube-based erbium fiber laser, *J. Opt. Soc. Am. B* **30**, 158 (2013).
- [41] A. Komarov, K. Komarov, and F. Sanchez, Quantization of binding energy of structural solitons in passive mode-locked fiber lasers, *Phys. Rev. A* **79**, 033807 (2009).
- [42] Y. Du, Q. Gao, J. Li, C. Zeng, D. Mao, and J. Zhao, Periodic attraction and repulsion within the tight-bound π -phase soliton molecule, *Opt. Lett.* **46**, 5599 (2021).

- [43] E. J. Meier, F. A. An, and B. Gadway, Observation of the topological soliton state in the Su–Schrieffer–Heeger model, *Nat. Commun.* **7**, 13986 (2016).
- [44] Z. Wen, B. Lu, X. Qi, C. Zhang, K. Wang, H. Chen, and J. Bai, Effects of spectral filtering on pulse dynamics in a mode-locked fiber laser with a bandwidth tunable filter, *J. Opt. Soc. Am. B* **36**, 952 (2019).
- [45] Z. Wen, K. Wang, H. Chen, B. Lu, and J. Bai, Stable-, period-N- and multiple-soliton regimes in a mode-locked fiber laser with inconsistently filtered central wavelengths, *Opt. Express* **28**, 28033 (2020).
- [46] B. W. Plansinis, W. R. Donaldson, and G. P. Agrawal, What Is the Temporal Analog of Reflection and Refraction of Optical Beams? *Phys. Rev. Lett.* **115**, 183901 (2015).
- [47] B. W. Plansinis, W. R. Donaldson, and G. P. Agrawal, Temporal waveguides for optical pulses, *J. Opt. Soc. Am. B* **33**, 1112 (2016).
- [48] M. Brotons-Gisbert, G. E. Villanueva, J. Abreu-Afonso, G. Serafino, A. Bogoni, M. V. Andrés, and P. Pérez-Millán, Comprehensive theoretical and experimental study of short- and long-term stability in a passively mode-locked solitonic fiber laser, *J. Lightwave Technol.* **33**, 4039 (2015).
- [49] X. Jin, G. Hu, M. Zhang, Y. Hu, T. Albrow-Owen, R. C. T. Howe, T.-C. Wu, Q. Wu, Z. Zheng, and T. Hasan, 102 fs pulse generation from a long-term stable, inkjet-printed black phosphorus-mode-locked fiber laser, *Opt. Express* **26**, 12506 (2018).